Proceedings of the Twenty-first (2011) International Offshore and Polar Engineering Conference
Maui, Hawaii, USA, June 19-24, 2011

ISBN 978-1-880653-96-8 (Set); ISSN 1098-6189 (Set); www.isope.org

Numerical Simulation of Tsunami Generation by the Potential Flank Collapse of the Cumbre Vieja Volcano

Stéphane Abadie

Laboratoire SIAME,
Université de Pau et des Pays de l'Adour
Anglet, France

Department of Ocean Engineering,
University of Rhode Island,
Narragansett, USA

Jeffrey Harris and *Stéphan Grilli*
Department of Ocean Engineering, University of Rhode Island
Narragansett, USA

ABSTRACT

We perform numerical simulations of wave generation by the potential flank collapse of the Cumbre Vieja Volcano (CVV; La Palma ,Canary Islands, Spain). Subaerial slide scenarios are first defined based on recent slope stability studies of CVV; the identified scenarios have smaller volumes than those proposed by Ward and Day (2001), in the pioneering work that triggered the interest of the research community for CVV. Simulations of tsunami sources are performed using the previously validated (Abadie *et al.*, 2010) 3D incompressible multi-fluid Navier-Stokes model THETIS. Both 2D and 3D simulations (the latter using a cylindrical mesh) are performed, which investigate near field wave generation. Results show that a slide of 60-70 km^3 would have very significant consequences, at least for la Palma and other surrounding islands. Far field waves (tsunamis) are simulated in the 2D horizontal, fully nonlinear and dispersive, Boussinesq model FUNWAVE, which is initialized with the 3D Navier-Stokes solution. Results of preliminary tests are shown in the paper and more results will be presented at the conference.

KEY WORDS: Tsunami; wave; landslide; Navier-Stokes; VOF; Boussinesq; Volcano collapse; La Palma.

INTRODUCTION

Since the pioneering, but controversial, work of Ward and Day (2001), the potential flank collapse of the Cumbre Vieja Volcano (CVV) on La Palma island (Canary Islands, Spain; Fig. 1) has been the object of numerous studies of the related tsunami hazard. Ward and Day assumed an extreme scenario for the western flank collapse, involving a volume of about 500 km^3. Their simulations resulted in extremely large local waves, which reached still up to a 20 meters elevation, in the far field off of the US East coast (particularly in Florida).

This catastrophic landslide scenario was severely criticized (e.g., Mader, 2001; or Pararas-Carayannis, 2002) as well as the wave modeling approach used in the work. Masson *et al.* (2002, 2006) later found evidences of past large paleo-submarine landslides of O(100 km^3) volume, around the canary islands, at least demonstrating that such events were not purely speculative. However, turbidite deposits indicate that such large slides may have occurred in a retrogressive way, which would have reduced their tsunamigenic potential. From the geological point of view, however, one also needs to explain the abnormally high elevation of ancient marine sediment deposits found in the path of Ward and Day's calculated waves (McMurtry *et al.*, 2007), which would be consistent with a large tsunami.

Hence, if on the one hand the alarming work of Ward and Day (2001) may be subject to critics, on the other hand, one also must admit that there is a lack of knowledge regarding such kinds of extreme natural hazards and related physical phenomena.

While geological scenarios and landslide rupture mechanisms may still be subjects to conjectures, once a scenario is selected, significant recent progress made in landslide tsunami simulation, through using new advanced computational methods (e.g., Abadie *et al.*, 2010), make it possible to more realistically simulate wave generation by such violent subaerial (or submarine) mass failures. Indeed, owing to the complex geometry of the slide and the turbulent nature of the flow induced by such violent geophysical processes, initial tsunami generation simulations must be based on a three-dimensional (3D) Navier-Stokes (NS) model, that can account for multiple fluids (air, water) and materials (rock slide). Along this line, Løvholt *et al.* (2008) recently used a multi-material compressible fluid NS model to re-analyze wave generation for Ward and Day's original idealized slide scenario. The NS solution (Gisler *et al.*, 2006) was then used to initialize a Boussinesq long wave model (BM), to simulate the tsunami transoceanic propagation stage. Løvholt *et al.*'s results confirmed that dispersive effects are important for a realistic description of the far field, as expected for landslide tsunamis, due to their relatively shorter wavelength as compared to co-seismic tsunamis (e.g., Watts *et al.*, 2003, Grilli and Watts, 2005; Enet and Grilli, 2007; Tappin *et al.*, 2008). This justified using a BM model, rather than a more standard non-dispersive long wave model, as was suggested earlier for landslide tsunami modeling (e.g., Watts *et al.*, 2003) or even, more recently, for analyzing dispersive effects and constructive interferences in the tail of co-seismic tsunamis (e.g., Grilli *et al.*, 2007; Ioualalen *et al.*, 2007; Grilli *et al.*, 2010). Note, for completeness, that a CVV flank collapse

tsunami propagation case study was performed by Grilli *et al.* (2006) and Pérignon (2006), using a BM model, but a simpler empirical subaerial tsunami source (Walder *et al.*, 2003); the proprietary nature of this work had prevented its publication until recently. Even though less catastrophic than Ward and Day's, Løvholt *et al.*'s simulations still predicted very significant wave elevations off of the US East coast.

In this work, we report on the application of an incompressible multi-fluid 3D-NS Volume Of Fluid (VOF) model (referred to as THETIS; e.g., Abadie *et al.*, 2010) to studying potential tsunamis caused by the CVV flank collapse. THETIS' ouputs are used as an initial condition for the (fully nonlinear and dispersive) Boussinesq model (FUNWAVE), in its more recent spherical and parallelized implementation (Kirby *et al.*, 2009). This work is intended first to revisit and possibly confirm Løvholt *et al.'s* simulations, using different models for tsunami generation and propagation, and a higher resolution resolution of the bathymetry. It is also aimed at providing additional physical insight into the generation and propagation processes, yielding a more comprehensive risk assessment, by simulating several slide scenarios based on new slope stability studies of the CVV flank (Fabre *et al.*).

Fig. 1: Cumbre Vieja Volcano (CVV), in La Palma (Canary Islands).

TSUNAMI GENERATION MODEL

THETIS is a multi-fluid NS solver developed by the TREFLE CNRS laboratory at the University of Bordeaux. It is a multi purpose CFD code, freely available to researchers (http://thetis.enscbp.fr). [Note, however, so far the code documentation is only available in French.] In this section, we give a summary of the application of THETIS to landslide tsunami modeling. More details in this respect, as well as a thorough validation of THETIS for 2D and 3D rigid slide cases, can be found in Abadie *et al.* (2010).

THETIS solves the incompressible NS equations for water, air and the slide (considered in this study as a Newtonian fluid, but this is not a limitation as other rheological models could be used). Basically, at any time, the computational domain is considered as being filled by one "equivalent" fluid, whose physical properties (namely density and viscosity) vary with space.

The governing equations (i.e., conservation of mass and momentum) are discretized on a fixed mesh, which may be Cartesian, cylindrical or curvilinear, using the finite volume method. These governing equations are exact, except for interfacial meshes, where momentum fluxes are only approximated, due to the presence of several fluids. In the present work, subgrid turbulent dissipation is modeled based on a Large Eddy Simulation approach, using a mixed scale subgrid model (Lubin *et al.*, 2006). NS equations are solved using a two-step projection method. All fluid-fluid interfaces are tracked using the VOF method. Once, the velocity field is known, fluid volume fractions are advected using the TVD scheme, which keeps numerical diffusion bounded.

SLIDE SCENARII

Slope stability studies along the western flank of the CVV were performed as part of the European research project TRANSFER (Fabre *et al.*, in revision; see also Abadie *et al.*, 2008). The 2D geometrical model (in a vertical plane), for a potential flank collapse and the location of the failure surface were inferred from field data, laboratory tests, and slope stability analyses performed using two different numerical models based on a Mohr-Coulomb failure criterion..

By gradually decreasing material property values (thus mimicking hydrothermal alteration), the potential failure surface was identified. A global shear zone, more or less parallel to the topography and dipping 24° westward, was found based on global plastic indicators and areas of maximum shear strain. Identification of a 2D slide cross-section finally allowed determining slide volume from field data (width and length of semi-elliptic shape). Following this approach, Fabre *et al.* estimated potential CVV landslide volumes ranging between 38 and 68 km^3, depending on the hypotheses made to assess the lateral extent of any given failure. These values, which are smaller than those proposed earlier by Ward and Day (2001) (500 km^3) or used in Gisler *et al.* (2006) and Løvholt *et al.* (2008), appear to be more reasonable, in view of the size of deep water deposits identified at the toe of the volcano, as possibly corresponding to its last massive flank collapse (about 300,000 years ago). Hence, these values will be considered in the present studies, but the 500 km^3 scenario will still be simulated to compare with Løvholt *et al.'s* (2008) results. Note, however, that the high safety factors found in Fabre *et al.*'s analyses indicate that the CVV's western flank is rather stable under present conditions. Large seismicity and/or a volcanic eruption could nevertheless provide additional destabilizing forces that were not included in their analyses.

2D LANDSLIDE TSUNAMI STUDY

The first numerical simulations were carried out in 2D. The objectives of this preliminary study were to : (i) more easily identify the optimized mesh, which will be then extended in 3D; (ii) investigate physical processes in a relatively simple configuration.

Thus, Fig. 2 shows the initial condition used in THETIS to simulate a 2D CVV flank collapse case. The computational domain (not entirely represented in Fig. 2) is 150 km long and 8 km deep. La Palma's bathymetry was obtained by digitalizing marine charts published in Masson *et al.* (2002), based on multibeam surveys carried out in 1997. Errors made during the digitalization process were estimated in the range $\pm$500 m, which would give a global resolution of about 1 km, to be compared to the 2 minute resolution (~3,700 m) of E-TOPO2 data previously used in Løvholt *et al.* (2008). The slide rupture surface is defined as the intersection of an ellipse, whose characteristics are given by the slope stability analysis, with the digital terrain model; the area of this rupture surface is 8 km^2.

In the model, solid boundaries are represented as porous media (with zero porosity). The slide is an inviscid fluid with a 2500 kg/m^3 density. Free surface elevations are calculated at three off-shore locations.

Fig. 2 : Initial conditions for Thetis 2D simulations. Numerical gages G1, G2, G3 (not represented here) located respectively 10 km, 45 km and 100 km off shore.

As NS simulations are computationally demanding, the 3D mesh must be carefully defined to ensure sufficient accuracy and convergence, for the smallest possible grid size. Such grid selection thus requires several trial and error simulations to be run, which are more easily undertaken in 2D. The choice of a mesh able to correctly reproduce landslide tsunami generation processes is not straight-forward. This is mainly due to the fact that, after generation, waves and landslide do not follow the same trajectories and, especially in 3D, the wave field spatial extent rapidly grows with time.

As a first step, we limit 2D simulations to the generation area, with a computational domain only extending to 30 km off shore. Several meshes are considered, all involving square meshes, with grid steps (i.e. $\Delta x=\Delta z$) ranging from 250 to 40 m. Fig. 3 shows waves computed at gage G1 (Fig. 2; 10 km from the shoreline), for three different grid step sizes. In 2D, the wave height reaches about 1,000 m at this location; this large value results in part from the reduced spatial energy spreading in 2D, as compared to 3D. The signal does not show much dependency to grid step, indicating that convergence in terms of free surface elevation is quite easily achieved at least in the generation area.

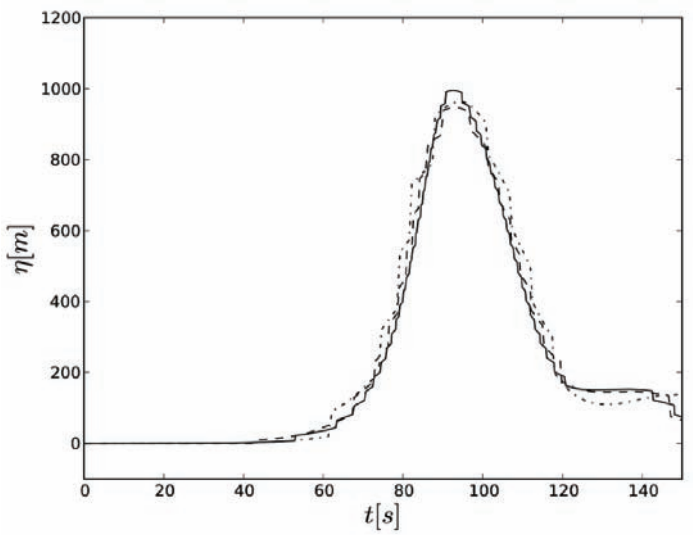

Fig. 3 : Free surface time history (case of Fig. 2) at gage G1 (Fig. 2; 10 km off-shore) for three meshes : mesh 1 (solid line) $\Delta x=\Delta z$=40m, mesh 2 (dashed line) $\Delta x=\Delta z$=100m, mesh 3 (dot-dashed line) $\Delta x=\Delta z$=200m.

We next assess wave propagation computations in a larger domain, extending to 150 km offshore. Our reference solution is calculated using a constant grid step $\Delta x=\Delta z$=100 m. This solution is improved by refining the mesh around the free surface (minimum vertical grid step Δz_{min}=10 m); 120 meshes are used in the vertical *z* direction and 1,500 in the horizontal *x* direction. The wave train computed at gages G1, G2 and G3 using this fine mesh is plotted as solid lines in Fig. 3; the dispersive nature of the generated wave train is apparent on the figure.

Such a high resolution grid, however, is too fine to be used in full 3D computations. Instead, we will attempt to reproduce the 2D finer grid solution using a coarser irregular 3D grid, defined as an exponentially growing grid, featuring 200 meshes in the horizontal *x* direction and starting at the rightward boundary with a minimum size Δx_{min} = 200 m. In the *z* direction, the grid is reduced to 80 meshes, with a constant step of 100 m.

This irregular mesh is first tested for 2D computations, and Fig. 3 shows the free surface computed at the three earlier gages. Although differences occur with the finer mesh, these are quite small, indicated that this relatively coarser mesh is adequate for 3D computations to achieve sufficient convergence and accuracy of the results. It should be noted that slightly improved results could be obtained by refining the grid around the free surface. Such 3D computations, which are still ongoing, will be presented at the conference.

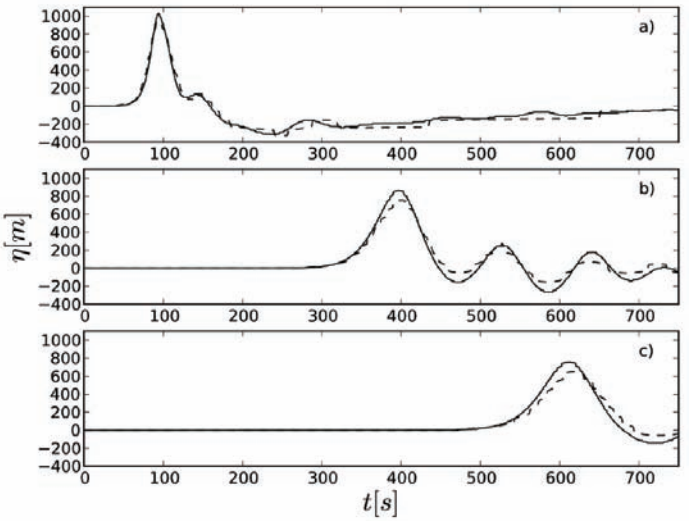

Fig. 4 : Free surface time history (case of Fig. 2) at gage : a) G1 (10 km off-shore), b) G2 (45 km off-shore) and c) G3 (100 km off-shore) for two meshes : mesh 1 (solid line) 1500x120 (Δx=100 m, irregular in z), mesh 2 (dashed line) 200x80 (irregular in x and regular in z).

Co-seismic tsunamis generally feature long wavelengths, with relatively small wave height (order of meters). Even though in this particular event, generated waves are much higher, the relatively low resolution in the *z* direction (in both grids) may still pose a problem. Thus, with Δz = 100 m, one would expect the result's accuracy to be at best about 2 or 3 times this length (i.e. 200-300 m). The following test, however, shows that this is not the case and that a better resolution can be expected in the results. To verify this, we ran 2D simulations of linear intermediate depth waves, in a periodic domain in the *x* direction. Free surface elevation and water velocities were specified as initial conditions based on linear wave theory. The computational domain is 10 m long, 2 m high and the still water depth is h = 1.3 m. The mesh is constant in the *z* direction with a vertical grid step of 2 cm (i.e. 1/65 the depth). The wave period is T = 3.084 s and the wave amplitude is set to: 3, 1.5 and 1 cm, in three different tests, respectively. With these parameters, the linear dispersion relationship yields a wavelength L = 10.00 m, which is exactly the selected domain length.

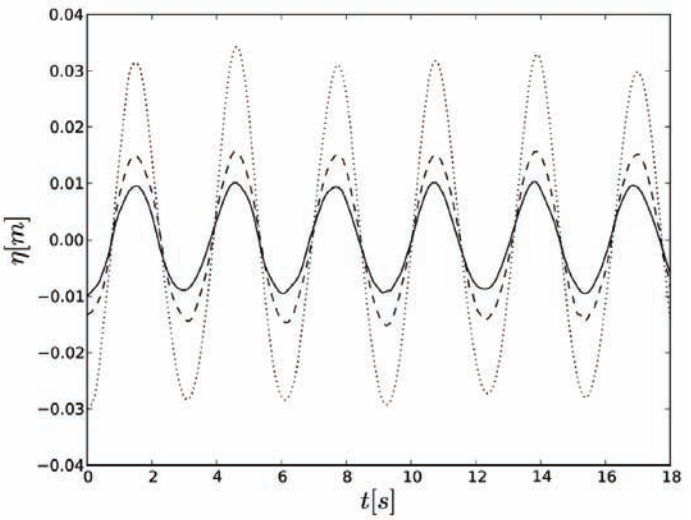

Fig. 5 : linear wave propagation computed with a regular grid mesh (Δz = 2 cm). Free surface time history at x = 5 m. Wave amplitudes are: 1 cm (solid line), 1.5 cm (dashed line) and 3 cm (dotted line).

Fig. 5 shows the free surface elevation computed at $x = 5$ m, at the half-length of the domain. Wave amplitudes and periods remain stable over the 5 wave period range of the simulation shown on the figure, indicating that waves of lower amplitudes than the model vertical resolution may be accurately simulated.

Fig. 6 shows a sequence of density contours computed at four time steps using the mesh 1 of Fig. 4. Initial conditions correspond to Fig. 2. As depicted in this sequence, the slide flows as a thin fluid sheet with a bulbous shape front. Several major water waves are created (see also Fig. 4b), with the first wave being the highest. As seen on Fig. 6, a small amount of slide material stays trapped at the basis of the elliptical cavity. We shall see that this also happens in 3D simulations and appears difficult to avoid. At the end of the simulation, the actual slide volume has to be recalculated by substracting the amount of trapped slide material.

The evolution of slide velocity is plotted on Fig. 7a. A maximum slide velocity of about 150 m/s, to be compared to the 190 m/s found in Løvholt *et al.*, 2008, is reached after an acceleration time of around 100 s. Then the slide maximum velocity, which appears to occur within the second left half of the slide, progressively decreases, while keeping a significant magnitude. The velocity is significantly non-uniform within the slide fraction, as shown by the significantly lower value of the mean velocity.

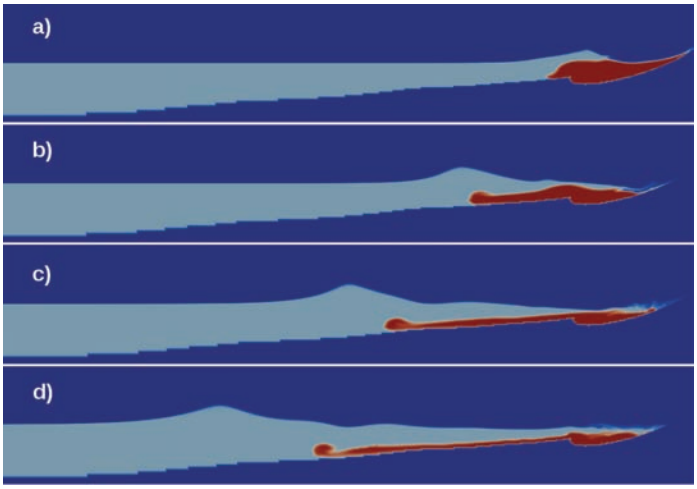

Fig. 6 : Density contours at : a) t=50 s, b) t=100 s, c) t=150 s, d) t=200 s. 2D simulation of Fig. 2,3,4 (slide initial surface equal to 8 km^2).

The slide local Froude number (i.e., $v_{slide}/\sqrt{gh_{loc}}$) time evolution is plotted in Fig. 7b, up to 170 s (which is the time of the highest free surface deformation, see Fig. 6c). The slide flow is slightly supercritical and becomes subcritical after this time. For such Froude number values, around 1 for a long time, the wave generation process is very efficient and, as a consequence, the maximum free surface elevation is very important (Fig. 7c).

The simulation shows two clearly distinct flow zones, each located on one side of the slide tip. Downstream of the slide tip, the flow field exhibits water waves propagating from right to left. Upstream (Fig. 8), shorter water waves propagate along with a strong rightward current (~20 m/s), which affects the whole water column, from the slide tip to the initial slide cavity. This limit between the two zones is moving with the slide velocity and the flow pattern lasts until the end of the simulation (~1,300 s). This current is generated to balance the slide mass input into the undisturbed water body, allowing water to fill the gap left upstream by the slide. As in Løvholt *et al.* (2008), we note the occurrence (Fig. 8) of multiple vortices at the interface between slide and water, which we attribute to Kelvin-Helmholtz instabilities.

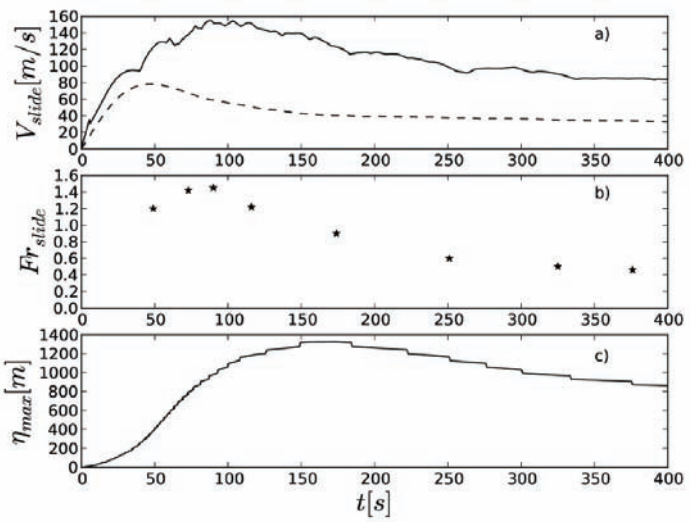

Fig. 7 : Same case as Fig. 6. a) (solid line) slide maximum velocity, (dashed line) slide mean velocity, b) slide local Froude number, c) maximum free surface elevation, versus time.

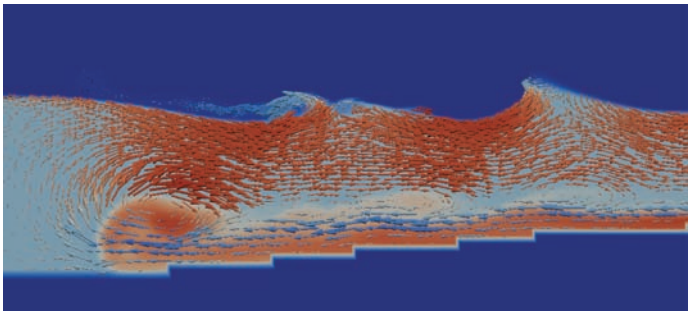

Fig. 8 : Same case as Fig. 6. Detailed velocity field around the slide tip at t=438 s, showing the strong current generated in the water by the slide displacement.

3D SIMULATIONS

3D computations have been carried out in a cylindrical mesh to better resolve the radial nature of wave propagation. Thus, the computational domain is a cylinder of height 8 km and radius 150 km. Based on 2D simulations, this mesh features 200 grid cells in the radial r direction (irregular spatial steps, with Δr_{min}=200 m in the initial slide area), 80 grid cells in the vertical z direction (constant spatial step Δz=100 m) and 200 grid cells in the θ direction (constant spatial step $\Delta\theta$=1.8 °).

Four slide scenarios were considered for this study, with initial slide volumes of : 80 km^3 or 40 km^3, consistent with the results of the slope stability analyses (Fabre *et al., in revision);* a 20 km^3 lower case and the 450 km^3 extreme case similar to the scenario studied by Ward and Day (2001) and Løvholt *et al.* (2008). The latter last case being still running at the time we write this paper, only preliminary results will be reported here (Fig. 11), and more details will be presented at the conference.

Except for the 450 km^3 case, slide initial geometry is obtained by

taking the intersection between an ellipsoid and the digital terrain model. The largest length of the ellipsoid is North-South directed, the two other axes of the ellipsoid are inclined of 17 ° respectively versus vertical and horizontal direction. The slide mass center is 500 m above sea water level and located 2.5 km west and 12 km north of La Palma southern cape. For the 80 km^3 case, the ellipsoid axes were respectively a=8 km, b=4.5 km (width) and c=900 m (high), for the 40 km^3 case, a=7.5 km, b=4 km and c=600 m. Last for the lower 20 km^3 case, a factor 0.70 was applied on each axis length (with regards to the 40 km^3 case).

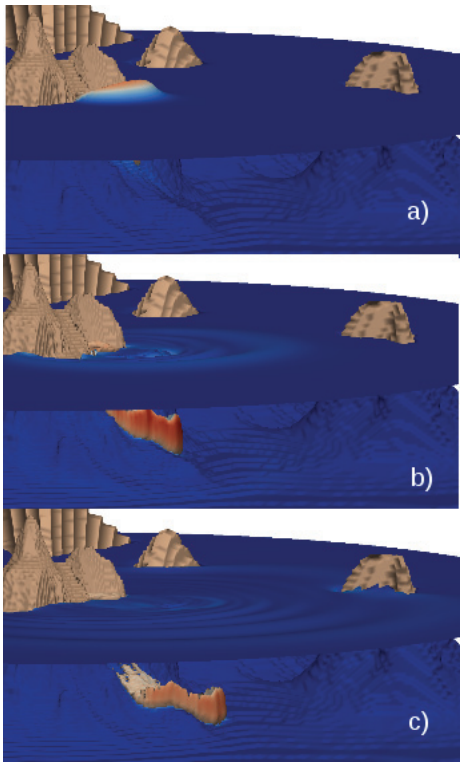

Fig. 9 : Snapshots of water and slide interfaces (volume fractions respectively equal to 0.5 and 0.1) at t=: a) 2 min, b) 6 min, c) 10 min into the event, with a slide initial volume of 80 km^3.

Fig. 9 shows snapshots of the numerical results for the 80 km^3 slide case. The vertical *z* coordinates have been exaggerated by a factor of 10, to allow for a better view of the wave field and slide motion. Besides La Palma island, which appears on the left front part of the picture, three other Canary Islands are included in the computation, (from right to left) El Hierro, La Gomera and Tenerife (the latter being obviously under-resolved by the cylindrical mesh).

The water and slide interfaces are displayed by plotting their respective volume fractions. Mixing of slide material and water occurs, due to strong shear between both phases. This process, which happens in real events, is here only approached in the computations, by means of numerical diffusion in the VOF advection equation. In Fig. 9, the contour corresponding to a slide volume fraction of 0.1 is plotted, which allows to follow the slide path and deformation. This value was chosen (rather than 0.5) because, due to strong mixing, a 50 % slide presence rate does not exist any more beyond some time of slide displacement. Regarding slide deformation, the bulbous shape taken by the slide front in 2D is similarly observed in this 3D case.

The slide motion first generates a large wave (Fig. 9a) followed by a few smaller trailing waves. As in 2D, the slide Froude number quickly reaches a maximum value around 1 (Fig. 9a), which then progressively decreases, the waves then propagating faster than the slide (Figs. 9b and c). Above the slide, the water free surface is perturbed by short waves. Like in the 2D case, a strong current moves water on-shore to fill the gap left by the slide.

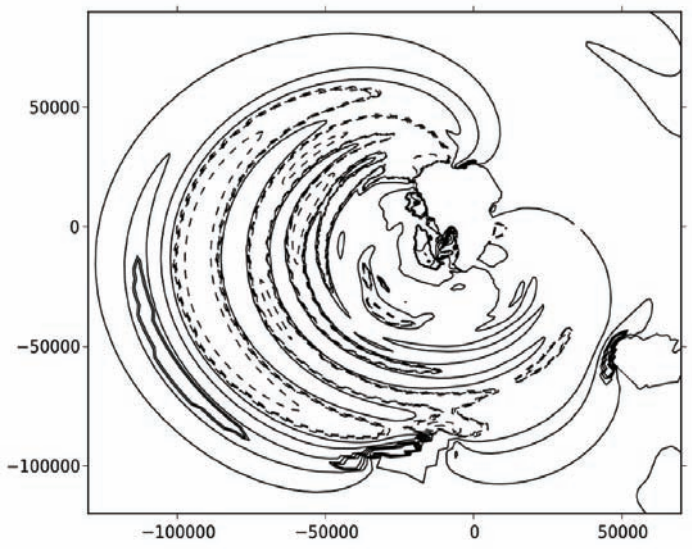

Fig. 10 : Free surface elevation after ~10 min (*t*=634 s). Contour step equal to 20 m. Positive elevations as solid lines (including 0) and negative elevations as dashed lines. Slide initial volume: 80 km^3.

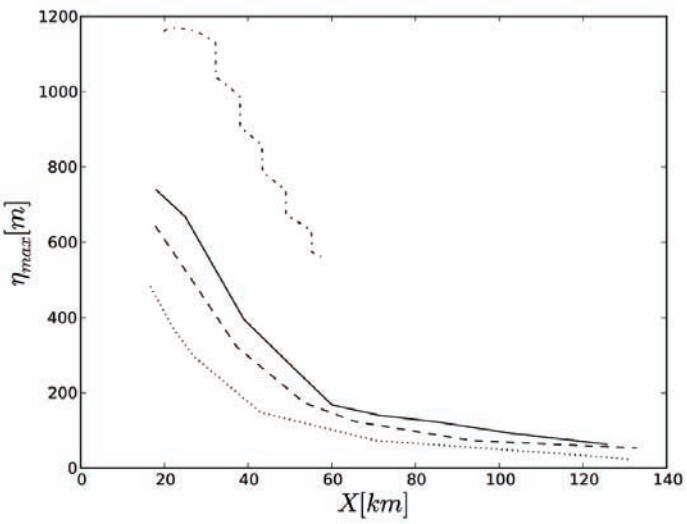

Fig. 11 : Computed decay of the maximum elevation of the first wave for a slide volume equal to : 20 km^3 (dotted line), 40 km^3 (dashed line), 80 km^3 (solid line) and 450 km^3 (dot-dashed line, run still ongoing).

Fig. 10 shows a plot of the free surface elevation after 10 min, for the 80 km^3 slide scenario. At this time, the wave train is composed of four waves, the largest first one having a maximum elevation of about 80 m and a through of -80m. The most energetic part of the tsunami is directed about 30° southward of the West direction. From this direction to the Westward one, the maximum elevation decreases from 80 to 50 m. The wavelength of the first wave is 30 km and its average celerity since its generation is 170 m/s. This value is consistent with the long wave celerity (~200 m/s in 4000 m depth), the difference being

attributed to the generation region, involving lower depths.

The free surface elevation increases strongly close to the Islands of El Hierro and Gomera, due to shoaling effects. In the North part of El Hierro, waves reach about 100 m elevation, while it is only about 40 m slightly West of the Island in deeper water areas. After turning around La Palma Island, a wave about 20-30 m high propagates eastwards.

The four slide scenarios simulated give a better understanding of the influence of the source geometry on tsunami features. For each case, the wave pattern is comparable to that shown in Fig. 10 at the same time, but wave elevations are significantly different. Fig. 11 shows the decay of the first wave elevation with the propagation distance. The curves only start when the maximum value is recorded. In each case, this maximum value is quickly reached after the slide triggering and then remains constant over a short period before starting to decay.

The maximum wave elevation calculated is 470 m, 633 m, and 750 m for the 20 km^3, 40 km^3, and 80 km^3 cases, respectively. Between a distance of 20 and 60 km, the decay of the first wave is found to be very fast (e.g., 14m/km for the 80 km^3 case). Beyond 60 km, this decay rate seems to decrease at least for the first three scenarios. After 120 km of propagation, the maximum wave elevation is 32 m, 50 m and 70 m for the 20 km^3, 40 km^3, 80 km^3 cases, respectively. The 450 km^3 scenario corresponding to Ward and Day's (2001) and Løvholt *et al.*'s (2008) scenario, is found to produce a maximum surface elevation of 1,170 m. After 60 km of propagation, the elevation is still about 550 m, which expectedly in view of the large slide volume is much larger than for the other scenarios.

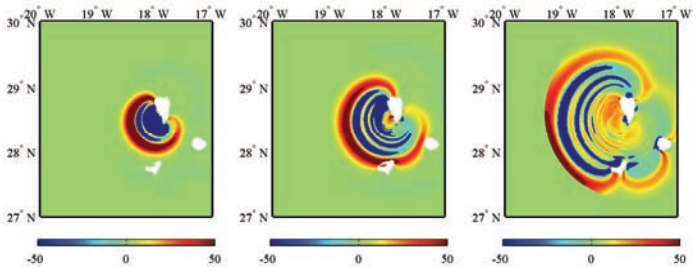

Fig. 12 : THETIS results for surface elevation (color scale in meter) at t= 360 s, 517 s, and 770 s (left to right), as interpolated onto the regional, 2 arc-second grid used for FUNWAVE computations.

BOUSSINESQ PROPAGATION MODEL

We now investigate the far field consequences of CVV's potential event. To do so, we use the fully nonlinear and dispersive Boussinesq model FUNWAVE (e.g., Wei *et al.*, 1995; Wei and Kirby, 1995; Chen *et al.*, 2000; Kennedy *et al.*, 2000) to model both the regional and trans-Atlantic propagation of the tsunami, whose source is generated using THETIS as detailed above. For ocean basin scale propagation, FUNWAVE is used in its latest spherical coordinate implementation, which also includes Coriolis effects (Kirby et al., 2009). Unlike the Nonlinear Shallow Water (NSW) equations, traditionally used for studying tsunamis, the Boussinesq approach includes dispersive effects that may be significant for landslide tsunami sources and affect tsunami propagation and runup through wave-wave interactions. FUNWAVE can also simulate both wave breaking and inundation over dry land.

Model setup

To initialize FUNWAVE, both the wave height and depth-averaged velocity computed with THETIS at a specific time (e.g., Fig. 12), are interpolated on FUNWAVE 2D spherical coordinate grid using triangle-based cubic interpolation. In the latter, all points outside of the Thetis mesh are assumed to have zero wave height and velocity.

The bathymetry used in FUNWAVE is obtained from the E-TOPO1 data, again, using cubic interpolation to obtain the regional bathymetry near and around La Palma, and subsampling it to obtain the North Atlantic grid. The regional grid near La Palma, in which the source is first interpolated, has 1,936 x 1936 grid cells, with a resolution of 15 arc-seconds (about 450 m), and is centered on 18.5 W, 28.5 N, and the North Atlantic grid has 2,401 x 1,201 grid cells, and extends from 85 W to 5 W, and from 10 N to 50 N, with a 2 arc-minute resolution (Fig. 13).

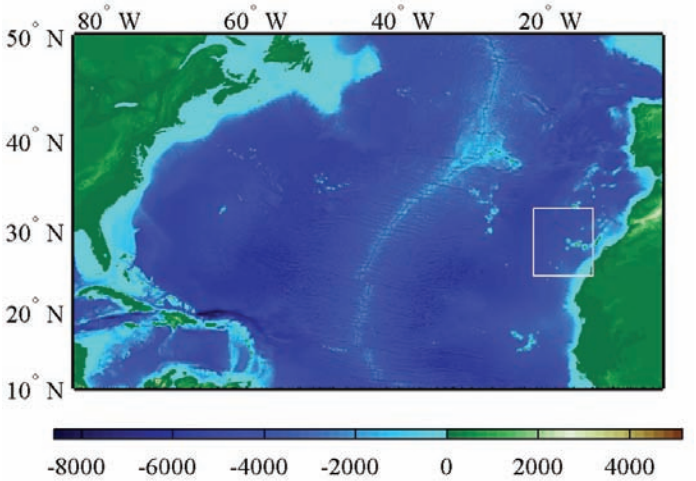

Fig. 13 : Bathymetry of North Atlantic, showing the grid used for trans-Atlantic propagation (2 arc-minute resolution), as well as the smaller, regional grid (white rectangle; 15 arc-second resolution).

Initialization testing

Similar to Lovholt *et al.* (2008), who used depth-averaged quantities to initialize their multimaterial code SAGE for tsunami simulations, we use depth-averaged quantities computed from THETIS' results in the same way. It is clear, however, that THETIS must simulate landslide tsunami generation for a sufficiently long time for the initial leading tsunami waves to satisfy the long-wave approximation. At the same time, THETIS' simulations of wave generation should not be too long as to become computationally prohibitive. Hence, to estimate the proper initialization time for FUNWAVE, we use THETIS' results for initialization at three different times (i.e., t=360 s, 517 s, and 770 s; e.g., Fig. 12 for surface elevation), and use FUNWAVE to model waves up to the latest time (i.e., the third) for the first two initializations.

We see in Fig. 14 that all three results are relatively similar. While the result from THETIS at 770 s clearly shows some spurious waves, because the tsunami reaches the boundary of the cylindrical mesh by then, the leading waves of the tsunami from the other two initial conditions appear to be cleaner. Therefore, for testing further propagation with FUNWAVE, we will use the 517 s initial condition, as it is likely to be the most accurate. This is done in the next sub-section.

Trans-Atlantic propagation

As detailed above, FUNWAVE is initialized using THETIS' results computed at t=517 s. The model is first run for an additional 25 min. on the regional 15" grid. Over this time, the initial waves become much longer (Fig. 14), allowing these to be accurately resolved in the coarser 2' Atlantic basin grid. Note that most of the wave energy is in the leading waves of the tsunami (this is verified in calculations not

reported here), so that if the waves near La Palma are not accurately modeled by the Boussinesq approximation, this will not have much effect on the far-field tsunami propagation.

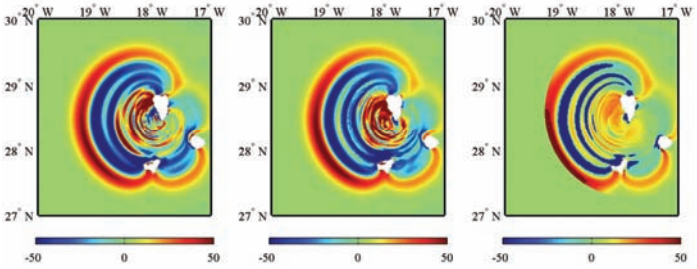

Fig. 14 : FUNWAVE results for surface elevation, for *t*=770 s, initialized by Thetis results computed at *t*=360 s (left), 517 s (center), and 770 s (right) (Fig. 12) and interpolated onto the regional FUNWAVE 15 arc-second grid.

After the additional 25 min. of simulated time in FUNWAVE, the results are re-interpolated on the 2' resolution grid covering the North Atlantic basin, and FUNWAVE is restarted.

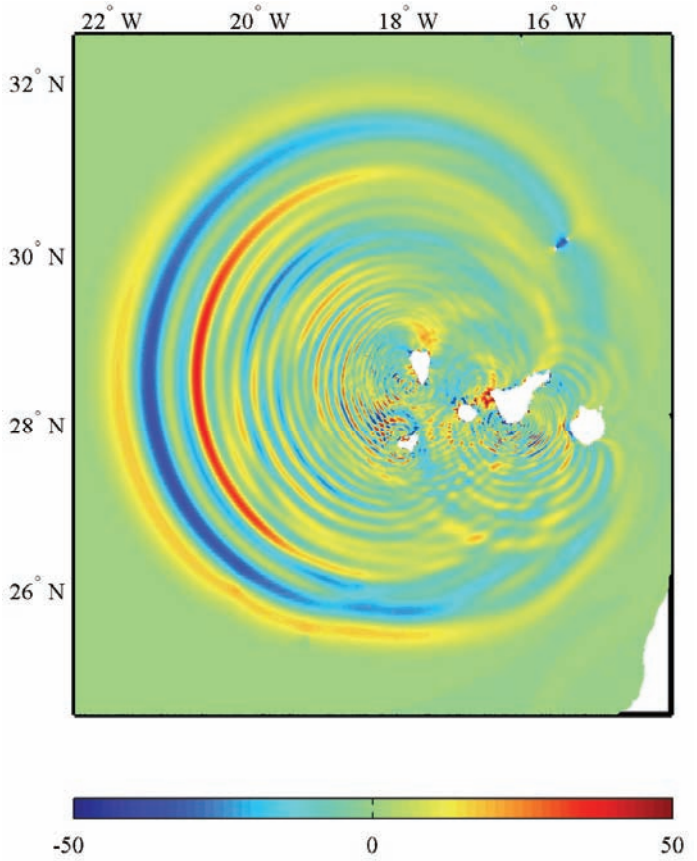

Fig. 15 : FUNWAVE results in regional 15" grid, at *t*=38 min, initialized at *t*=517 s with THETIS results (Fig. 12).

From the initial results presented here for the North Atlantic grid simulations (Fig. 16), we can clearly see how the leading edge of the tsunami wave train (which contains a few significant waves) propagates away from the shorter and more complex wave field, which can be seen near La Palma. It should be noted that there is a considerable amount of noise near the source region, in the 2' grid, that most likely is due to inaccuracies resulting both from the coarse resolution and the long-wave assumption, which does not hold very close to La Palma itself. But these are unlikely to have any effect on the leading waves of the far field tsunami. In future work, such side-effects of the simple coupling between THETIS and FUNWAVE can be filtered out in a more physically meaningful way.

Future work will mainly deal with investigating the far-field effects of such a tsunami event, including inundation and run-up along the East Coast of North America. The latter simulations will be performed in finer regional nested grids centered in the areas of largest tsunami impact identified in the coarse grid Atlantic basin simulations.

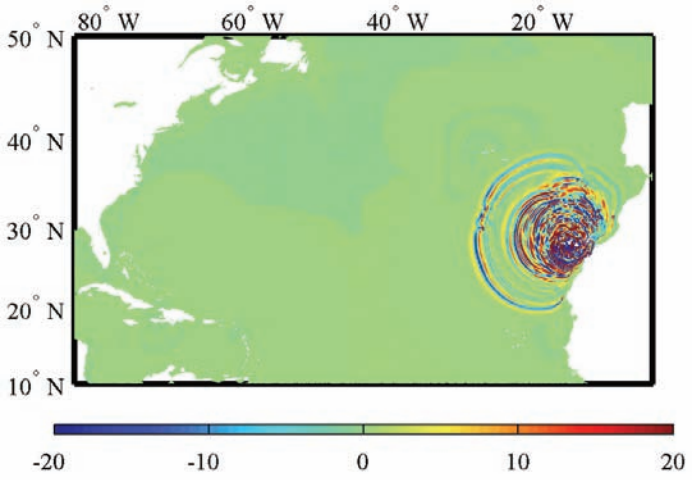

Fig. 16 : FUNWAVE results in the 2' North Atlantic grid, at *t*=93.6 min. (simulating the first 517 s with THETIS, the next 25 min. with FUNWAVE in the regional 15" grid, and the final 60 min. with FUNWAVE in the North Atlantic 2' grid).

CONCLUSIONS

An incompressible multi-fluid 3D Navier-Stokes model was used to simulate waves generated by the potential flank potential collapse of the Cumbre Vieja volcano. The NS solution was then used as input for the 2D long wave Boussinesq model FUNWAVE. The following main conclusions can be drawn from this work :

- Relatively coarse meshes are sufficient in THETIS to capture the wave physics, enabling reasonable 3D-NS simulations of initial subaerial landslide tsunami sources.
- Slide motion generates a strong reverse steady current in the water column.
- Slide scenarios with lower volume than Ward and Day's (2001) were devised based on recent slope stability studies. The selected 60-70 km^3 slide volume scenario still generate waves susceptible to induce very significant run-up values on the surrounding Islands and sizable far field tsunamis.
- The Navier-Stokes depth-averaged velocities and free surface elevations obtained after about 6-10 min simulations reasonably match long wave theory (for the leading waves) and thus can be used to initialize the Boussinesq model without producing significant errors

ACKNOWLEDGEMENTS

Partial funding for this work was provided by grant #NA10NMS4670010 of NOAA's "National Tsunami Hazards Mitigation Program (NTHMP)". Stéphane Abadie was awarded an Aquitaine Fulbright grant, cofunded by the Aquitaine Region and the Fulbright commission, during his stay at University of Rhode Island. Numerical simulations were run on a 12-core Mac Pro cluster located at

URI and funded by the NTHMP program, the 256 cores “elanion” cluster (ALTIX ICE 8200) cofunded by the Aquitaine Region and the 12288 cores “Jade” cluster of CINES. The authors also thank the “Institut de Mécanique et d'Ingénierie de Bordeaux” for the use of the “elanion” cluster and more specifically Stéphane Glockner for his support on technical and numerical aspects of THETIS model.

REFERENCES

Abadie, S, Grilli, S., Glockner, S., (2006), “A coupled numerical model for tsunami generated by subaerial and submarine mass failures”, *in Proc. 30th Intl. Conf. Coastal Engng.*, San Diego, California, USA. 1420-1431.

Abadie, S, Gandon, C., Grilli, S., Fabre R., Riss, J., Tric, E., Morichon D., Glockner, S. (2008), “3D Numerical simulations of waves generated by subaerial mass failures”. Application to La Palma case, *Proc. 31th Intl. Conf. Coastal Engng.*, 1384-1395, Hamburg.

Abadie, S, Morichon, D., Grilli, S., Glockner, S. (2008), “VOF/Navier-Stokes numerical modeling of surface waves generated by subaerial landslides”, *La Houille Blanche*, 1, 21-26.

Abadie, S., Morichon, D., Grilli, S., Glockner, S., (2010) “ A three fluid model to simulate waves generated by subaerial landslides”. *Coastal Engineering*, 57, 9, 779-794.

Chen, Q., Kirby, J. T., Dalrymple, R. A., Kennedy, A. B., and Chawla, A. (2000), "Boussinesq modeling of wave transformation, breaking, and runup. II: 2-D", *J. Wtrwy, Port, Coast, and Oc. Engrg.*, ASCE, 126, 1, 48–56.

Enet, F. and Grilli, S.T. (2007), “Experimental Study of Tsunami Generation by Three-dimensional Rigid Underwater Landslides”, *J. Waterway Port Coastal and Ocean Engineering*, 133(6), 442-454.

Fabre, R., Tric, E., Riss, J., Lebourg, T., Abadie, S. “New investigation of potential collapse of the Cumbre Vieja's volcanic edifice (La Palma Island; Spain); numerical evaluation of failure and estimated volume”. In revision.

Gisler, G., R. Weaver, and M. Gittings (2006), “SAGE calculations of the tsunami threat from La Palma”, *Sci. Tsunami Hazards*, 24, 288–301.

Goda, K. (1979), “A multistep technique with implicit difference schemes for calculating two- or three-dimensional cavity flows”, *J. Comput. Phys.* 30, 76–95.

Grilli, S.T., Baxter, C.D.P., Maretzki, S., Pérignon, Y. and Gemme, D., (2006), “Numerical simulation of tsunami hazard maps for the US East Coast, Technical Report of Year 1 *FMGlobal Project”*, 34 pps.

Grilli, S.T., Ioualalen, M, Asavanant, J., Shi, F., Kirby, J. and Watts, P. (2007), “Source Constraints and Model Simulation of the December 26, 2004 Indian Ocean Tsunami”, *J. Waterway Port Coastal and Ocean Engng.*, 133(6), 414-428.

Grilli, S.T., S. Dubosq, N. Pophet, Y. Pérignon, J.T. Kirby and F. Shi (2010), “Numerical simulation and first-order hazard analysis of large co-seismic tsunamis generated in the Puerto Rico trench: near-field impact on the North shore of Puerto Rico and far-field impact on the US East Coast”, *Natural Hazards and Earth System Sciences*, 10, 2109-2125, doi:10.5194/nhess-2109-2010.

Grilli, S.T. and P. Watts (2005), “Tsunami generation by submarine mass failure Part I: Modeling, experimental validation, and sensitivity analysis”, *J. Waterway Port Coastal and Ocean Engng.*, 131(6), 283-297.

Ioualalen, M., Asavanant, J., Kaewbanjak, N., Grilli, S. T., Kirby, J. T. and Watts, P. (2007), “Modeling the 26 December 2004 Indian Ocean tsunami: Case study of impact in Thailand”, *J. Geophys. Res.*, 112, C07024, doi:10.1029/2006JC003850.

Kennedy, A. B., Chen, Q., Kirby, J. T., and Dalrymple, R. A. (2000), "Boussinesq modeling of wave transformation, breaking, and runup. I: 1D", *J. Wtrwy, Port, Coast, and Oc. Engrg*., ASCE, 126, 1, 39–47.

Kirby, J. T., Pophet, N., Shi, F. and Grilli, S. T. (2009), “Basin scale tsunami propagation modeling using Boussinesq models: Parallel implementation in spherical coordinates”. In *Proc. WCCE-ECCE-TCCE Joint Conf. on Earthquake and Tsunami* (Istanbul, Turckey, June 22-24), paper 100 (published on CD).

Løvholt, F., G. Pedersen, and G. Gisler (2008), “Oceanic propagation of a potential tsunami from the La Palma Island”, *J. Geophys. Res.*, 113, C09026, doi:10.1029/2007JC004603.

Lubin, P., Vincent, S., Abadie, S. & Caltagirone, J.P., (2006), “Three-dimensional Large Eddy Simulation of air entrainment under plunging breaking waves”, *Coastal Engineering*, Volume 53, issue 8, .631-655.

Mader, C.L. (2001), “Modeling the La Palma landslide tsunami”, *Sci. Tsunami Hazards*, 19, 160.

Morichon, D., Abadie, S., (2010), “Vague générée par un glissement de terrain, influence de la forme initiale et de la loi de déformabilité du glissement”, *La Houille Blanche*, 1, 111-118, DOI: 10.1051/lhb/201001.

Masson, D., A. Watts, M. Gee, R. Urgeles, N. Mitchell, T. Le Bas, and M. Canals (2002), “Slope failures on the flanks of the western Canary Islands”, *Earth Sci. Rev.*, 57, 1 – 35.

Masson, D. G., C. B. Harbitz, R. B. Wynn, G. Pedersen, and F. Løvholt (2006), “Submarine landslides-processes, triggers and hazard prediction”, *Philos. Trans. R. Soc*., A364, 2009–2039.

McMurtry, G.M., Tappin, D.R., Sedwick, P.N., Wilkinson, I., Fietzke, J., Sellwoo (2007), “Elevated marine deposits in Bermuda record a late Quaternary megatsunami”, *Sedimentary Geol.*,200(3-4), 155-165.

Pararas-Carayannis, G. (2002), “Evaluation of the threat of mega tsunamis generation from postulated massive slope failures of island strato-volcanoes on La Palma, Canary Islands, and on the island of Hawaii”, *Sci. Tsunami Hazards*, 20, 251.

Pérignon, Y. (2006), Tsunami Hazard Modeling, *Senior Engineering Thesis.* Department of Ocean Engineering, University of Rhode Island and Ecole Centrale de Nantes, 40 pps.

Tappin, D.R., Watts, P., Grilli, S.T. 2008, “The Papua New Guinea tsunami of 1998: anatomy of a catastrophic event”, *Natural Hazards and Earth System Sciences*, 8, 243-266. doi:10.5194/nhess-8-243-2008.

Walder, J., P. Watts, O. Sorensen, and K. Janssen (2003), “Tsunamis generated by subaerial mass flows”, *J. Geophys. Res*., 108(B5), 2236, doi:10.1029/2001JB000707.

Ward, S. N. and Day, S. (2001), “Cumbre Vieja Volcano—potential collapse and tsunami at La Palma, Canary Islands”, *Geophys. Res. Lett*., 28, 397-400.

Watts, P., S. T. Grilli, J. T. Kirby, G. J. Fryer, and Tappin, D. R. (2003), “Landslide tsunami case studies using a Boussinesq model and a fully nonlinear tsunami generation model”, *Natural Hazards and Earth System Sciences*, 3, 391-402.

Wei, G. and Kirby, J. T. (1995), "Time-dependent numerical code for extended Boussinesq equations", *J. Wtrwy, Port, Coast, and Oc. Engng*., ASCE, 121, 5, 251-261.

Wei, G., Kirby, J. T., Grilli, S. T., and Subramanya, R. (1995), "A fully nonlinear Boussinesq model for free surface waves. Part I: Highly nonlinear unsteady waves", *J. Fluid Mech*., 294, 71-92.

.